frontiers | Frontiers in Earth Science

TYPE Original Research
PUBLISHED 10 August 2022
DOI 10.3389/feart.2022.983572



OPEN ACCESS

EDITED BY
Wenlong Ding,
China University of Geosciences, China

REVIEWED BY
Zhu Baiyu,
Yangtze University, China
Huigui Li,
Guizhou University of Engineering Science, China

*CORRESPONDENCE
Qirong Qin,
qqrong@126.com

SPECIALTY SECTION
This article was submitted to Structural Geology and Tectonics, a section of the journal Frontiers in Earth Science

RECEIVED 01 July 2022
ACCEPTED 18 July 2022
PUBLISHED 10 August 2022

CITATION
Fu L, Qin Z, Xie A, Chen L, Li J, Wang N, Qin Q and Mao K (2022), The relation of the "four properties" and fluid identification of the carboniferous weathering crust volcanic reservoir in the Shixi Oilfield, Junggar Basin, China. *Front. Earth Sci.* 10:983572. doi: 10.3389/feart.2022.983572



# The relation of the "four properties" and fluid identification of the carboniferous weathering crust volcanic reservoir in the Shixi Oilfield, Junggar Basin, China

Lei Fu[1], Zhangjin Qin[2], An Xie[3], Liang Chen[4], Junfei Li[1], Nan Wang[1], Qirong Qin[5]* and Kailan Mao[5]

[1]Shixi Field Operation District, Xinjiang Oilfield Company, CNPC, Karamay, China, [2]Exploration Division, Petro China Southwest Oil and Gasfield Company, Chengdu, China, [3]Evaluation Department of Xinjiang Oilfield Company, CNPC, Karamay, China, [4]Development Department of Xinjiang Oilfield Company, CNPC, Karamay, China, [5]School of Geosciences and Technology, Southwest Petroleum University, Chengdu, China

This study addresses the poorly understood physical properties of the Shixi Oilfield reservoir, which consists of a weathered Carboniferous volcanic rocks with strong heterogeneity and in which logging identification and evaluation are difficult. Using the lithology, lithofacies, and reservoir space characteristics of volcanic materials, this comprehensive study uses core, well logging, mud logging, and production testing data to analyze the relationship among the lithology, physical properties, electrical properties, and oil-bearing properties (referred to as the "four properties") of weathered Carboniferous volcanic crust in addition to fluid identification. 1) The lithology of Carboniferous volcanic crust is dominated by breccia lava, agglomerate, banded lava, and compact tuff, and the lithofacies are mainly effusive facies. Secondary pores and tectonic fissures are important reservoir spaces, and the corrosion-fracture pores are significant for reservoir properties. 2) The "four properties" of volcanic reservoirs in the study area have clear relationships. On this basis, data on the electrical properties of the material, such as interval transit time, density, and neutron, were used to establish a logging interpretation model of the properties and oil saturation of the volcanic rock. 3) Using the resistivity-porosity cross-plot method, normal probability distribution method, and Rt/Rxo-Rt cross-plot method, volcanic reservoir fluids were identified with coincidence rates of 80%, 63.63%, and 63.63%, respectively. The cross-plot method determines lower limits of the reservoir's physical properties and oil saturation, yielding porosity>9%, permeability>0.2 mD, and oil saturation>45%.

KEYWORDS

**"four properties" relation, fluid identification, lower limits of physical properties, logging interpretation model, weathering crust volcanic crust, carboniferous, Shixi Oilfield**

# 1 Introduction

Volcanic oil and gas reservoirs provide important avenues for oil and gas exploration and are widely distributed in more than 40 basins in 13 countries around the world. Compared with primary volcanic deposits, the reservoirs of weathered secondary volcanic rock have significantly better reservoir property and oil-gas productivity than primary volcanic reservoirs. This major new understanding has promoted the exploration and discovery of many of these reservoirs (Feng 2008; Fan et al., 2020a; Weng et al., 2020; Li, 2022; Li, 2018; Liu et al., 2022). The weathered volcanic crust reservoirs in the Junggar Basin of China are widely distributed. More than 40 such oil and gas reservoirs have been discovered successively in Hongshanzui, District 5, District 8, District 7, Chepaizi, Shixi, Huwan District, and other areas. In recent years, researchers have devoted themselves to studying volcanic eruption, reservoir characteristics, and the controlling factors and have achieved rich research results (Zou et al., 2012; Hou et al., 2013; Yang et al., 2017; Li et al., 2017).

Since the discovery of well Shixi 1 (hereafter SX1) in 1992, the Carboniferous volcanic reservoir in the Shixi Oilfield, a typical reservoir of weathered volcanic crust, has been built up as a modern desert oil and gas field. The Carboniferous stratigraphic structure in this area is complex, including small faults that developed with rapidly changing occurrences. The lithology is also complex, as the effective thickness is highly heterogeneous, and the oil-water transition zone is nonuniform, resulting in many oil-bearing well sections and large changes in oil layer thickness and testing effects. The development degree of the reservoir (on a plane) is uneven, influenced by many factors, such as anomalously high pressure, fracture development, and active bottom water, which seriously restrict the efficient development of the reservoir (Li et al., 2019, Li et al., 2020; Zhang et al., 2020; Li et al., 2021; Qie et al., 2021; Shan et al., 2021). Recently, relevant studies have been conducted on the geological characteristics of oil reservoirs in this area, mainly including the characteristics of single-well volcanic reservoirs, primary gas pores, and tectonic styles (Chen et al., 1999; Hou et al., 2012; Li et al., 2017). However, studies of the relationship among the four properties (including lithology, physical properties, electrical properties, and oil/gas properties) and fluid identification of the volcanic reservoirs in this area are sparse. Limited research is not conducive to understanding the distribution of remaining oil reserves or to oil and gas development and expansion. In general, the fluid identification of volcanic reservoirs is based on elementary methods, such as the three-porosity combination, ratio, cross-plot identification, standard stratum superposition, and others. In addition, some scholars also use statistical techniques, such as neural networks, to identify fluids. Since the lithology and lithofacies of volcanic deposits have a great influence on the logging response of fluid identification, starting with lithology and lithofacies, this study investigates the relations of the four properties in this region and conducts research on fluid identification of volcanic reservoirs.

# 2 Geological setting

Geographically, the Shixi Oilfield is in Karamay City, Xinjiang, China, and is structurally located in the Shixi uplift in the interior of the Junggar Basin. It is adjacent to the West Depression of well Pen 1, Sannan Depression, and Dishuiquan Depression to the south, north, and east, respectively, showing favorable geological conditions of being "Adjacent to the West Depression in three directions" (Figure 1A). The study area can be divided into three uplifts, two Depressions, and five structural units. From west to east, these units are well SX1 Uplift, well SX1 South Depression, well SX4 South Uplift, well Shimo 1 (hereafter SM1) West Depression, and well SM1 Uplift. Among them, the Carboniferous system in well SX1 Uplift has been entirely explored, of which oil and gas are the most abundant resources. The overall shape is a triangular horst bordering the north fault of well SX2, the west fault of well S002, and the south fault of well SM1. Its interior can be further divided into three secondary tectonic units, i.e., the east horst-block, the west fall-block, and the north fault stage (Figure 1B).

The strata encountered by drilling from the bottom to the top in the Shixi area are Carboniferous (C), Permian Jiamuhe Formation ($P_1j$), Wuerhe Formation ($P_2w$), Triassic Baikouquan Formation ($T_1b$), Ke Xia Formation ($T_2k^1$), Ke Shang Formation ($T_2k^2$), Baijiantan Formation ($T_3b$), Jurassic Badaowan Formation ($J_1b$), San Gonghe Formation ($J_1s$), Xi Shanyao Formation ($J_2x$), Cretaceous Tu Gulu Formation ($K_1t$), Tertiary (R) and Quaternary (Q) (Figure 1C) (Li et al., 2017; Li X. et al., 2022). The Carboniferous structure in Shixi is an ancient buried hill with an amplitude variation in the hill surface that gradually decreases from south to north. The structural high points are in the region of well SH1025-well SX1 in the east area and the region of well SH1120-well SH1059 in the west area. Ten reverse faults are developed in the region, of which the fault of northern well SX2 and the fault of southern well SX1 are reservoir-controlling faults. They clamp each other to form a fault-block buried hill structure of the Carboniferous in the Shixi area. On the seismic section, the fault characteristics are clear, and the fault displacement is large; the rest of the faults in the study area have small extension lengths without reservoir-controlling features (Table 1), and the vertical fault displacement is within 20 m, which further complicates the structure.

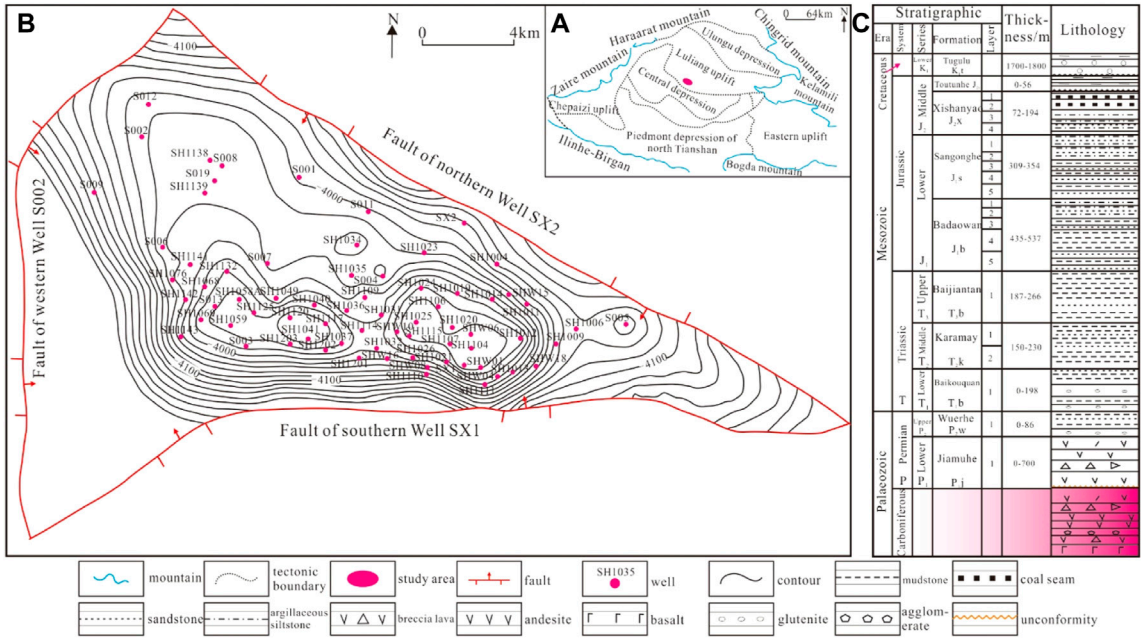


FIGURE 1
Geological survey of the study area. **(A)** Tectonic position; **(B)** The top surface structure of carboniferous; **(C)** Comprehensive stratigraphic histogram.

TABLE 1 Reservoir controlling fault (Type I fault) elements of Carboniferous volcanic rocks in Shixi Oilfield.

| Number | Fault | Fault properties | Length (km) | Disconnected horizon | Strike | Inclination | Dip (°) | Fault distance(m) |
|---|---|---|---|---|---|---|---|---|
| 1 | Fault of northern well SX2 | Reverse fault | 19 | T ~ C | NW | SW | 30–45 | 150 |
| 2 | Fault of southern well SX1 | | 23 | T ~ C | EW | N | 40–50 | 200 |
| 3 | Fault of western well S002 | | 14 | T ~ C | NS | E | 40–50 | 150 |

# 3 Samples and methods

## 3.1 Samples

The samples and data used in this study mainly include field measurements, cores, and thin-section observation. Analysis of the physical properties of the cores was also conducted. Field measurements include the conventional logging and production data for 15 wells. The conventional logging data were chiefly collected through natural Gamma-ray (GR), spontaneous potential (SP), borehole diameter (CAL), deep lateral resistivity (Rt), acoustic (AC), density (DEN), and neutron (CNL) methods, among others. The production materials mainly include testing, perforation, and production dynamics. Observed cores from 10 wells (e.g., SX1, SX2, S001, S002, S003, S004) of length 152.0 m, and 212 photos of cores and fractures were obtained. Ten such samples were obtained.

## 3.2 Methods

Laboratory experiments were carried out on core samples to obtain porosity and permeability data, and thin-section observations were conducted to study the lithology and lithofacies characteristics of Carboniferous volcanic reservoirs in combination with regional sedimentary and tectonic backgrounds. Combined with conventional logging and production test data, the four-property relationship, logging interpretation model, and fluid identification of reservoirs are studied. Three main methods were adopted for reservoir fluid

identification: the resistivity-porosity cross-plot method, the normal probability distribution method, and the Rt/Rxo-Rt cross-plot method. The second method is more complex and will be explained here. Parameter $P^{1/2}$ was adopted for drawing a map on the probability paper to identify oil and water strata and estimate Sw, a method called the "normal probability distribution method". Let P=Rt × Φm, where Rt is replaced by deep detection resistivity, Φ is obtained from porosity logging, and cementation index *m* can be estimated by using a statistical method (Pan et al., 2019; He et al., 2020; Ajaz et al., 2021). *p* values were calculated for each reservoir, and $P^{1/2}$ was plotted against the cumulative frequency on a probability paper. This method can convert an arc-shaped normal probability curve into a straight line. The larger the slope (k) of the straight line is, the smoother the normal probability distribution curve; in contrast, the normal probability distribution curve is more vertical and steeper. Therefore, the fluid identification of the method generally applies to the following rules: the slope of the oil and gas stratum is relatively large, while the slope of the water stratum is relatively small.

# 4 Results

## 4.1 Basic characteristics of the reservoir

### 4.1.1 Lithology and lithofacies characteristics

Combined with core, conventional logging, thin-section authentication, and other data, the Carboniferous volcanic materials in this area are divided into three sections, from bottom to top: basic-intermediate basic rocks (Section 1), intermediate rocks (Section 2), and intermediate-acid rocks (Section 3). These sections form a complete eruption cycle and include three categories: lava, ordinary pyroclastic rock, and transitional rock. Among these categories, lava is the most developed stratum and mainly includes andesite, rhyolite, dacite, and basalt, which is dominated by banded lava (Chen et al., 1999; Hou et al., 2012; Hou et al., 2013). Ordinary pyroclastic rocks mainly include agglomerate, agglomerate breccia, volcanic breccia, and breccia tuff. The agglomerate and agglomerate breccia are the most widely developed, and the breccia composition is mainly andesite. The transition rocks are mainly dacite and andesite transition rocks. On the whole, the lithology of the reservoir is primarily banded lava, agglomerate, breccia, compact tuff, and similar minerals, accounting for more than 84% of the deposits. The lithofacies include explosion facies and effusive facies, dominated by the effusive facies. Andesite and dacite of effusive facies are widely distributed, mainly in the west and east of the study area. In contrast, the andesite tuff breccia and dacite breccia of the explosion facies are mainly distributed in the area, such as well S008-well S013-well S004 (Figure 2).

### 4.1.2 Reservoir space types and characteristics

Pores and fractures are the most important reservoir space types in Carboniferous volcanic reservoirs (Fan et al., 2020b; He et al., 2021; Li J. et al., 2022). Pores include primary and secondary pores, with the secondary pores being more meaningful for oil and gas reservoirs. Primary blow holes and intercrystalline pores dominate the primary pores, but such pores often appear alone. Although these structures increase the porosity of the reservoir, the migration of oil and gas is hindered. Primary pores refer to the pores left by the loss of the volatile components after the magma is ejected and condensed on the surface. Most are circular or elliptical and mainly developed at the bottom and top of the lava flow (Figures 3A,B); the intercrystalline pores mainly refer to the pores inside the crystal grains of minerals, such as quartz and feldspar. These have irregular shapes, and the size of the pores is mainly positively correlated with the size of the particles (Figures 3C,D). The secondary pores are dominated by various dissolution pores, such as matrix dissolution pores, intergravel dissolution pores, intercrystalline dissolution pores, intragravel dissolution pores, and others. Such pores are the products of the dissolution minerals, often with unclear boundaries and extremely irregular shapes (Figures 3E,F).

Fractures can not only provide reservoir space but also connect those isolated pores, thereby effectively improving the seepage capacity of the reservoir. According to the observation of cores and thin sections, the fractures of Carboniferous reservoirs mainly include tectonic fractures, condensation shrinkage fractures, intergravel fractures, dissolution fractures, and others. Among these, tectonic fractures are the most developed. The tectonic fractures are formed under the action of tectonic stress, and their distribution range is wide and regular. Tectonic fractures can be divided into shear and tensile fractures based on their mechanical characteristics. Shear fractures are dominant, and their characteristics are different from those of tensile fractures (Figure 3K) (Kang 2021; Li et al., 2019a; Smeraglia et al., 2021; Wang and Wang 2021). They are characterized by strong distribution regularity, long extension length, obvious directionality, strong stratum penetration, and straight fracture surface (Figures 3G–J). Weathering fractures are formed by weathering and leeching and are affected by lithology, climate, terrain, and other factors. In general, they are short in length and lie within the stratum. Their fracture surfaces are slightly corroded, forming irregular shapes (Figure 3L). Condensation shrinkage fractures refer to the primary pores and shrinkage fractures formed during the formation of volcanic deposits and magma condensation diagenesis due to the change in facies and the decrease in volume, whereas intergravel (crystal) fractures refer to the small irregular fractures developed in the process of diagenesis, which cut through the gravel or only develop within the gravel. These fractures of different origins can connect the primary and

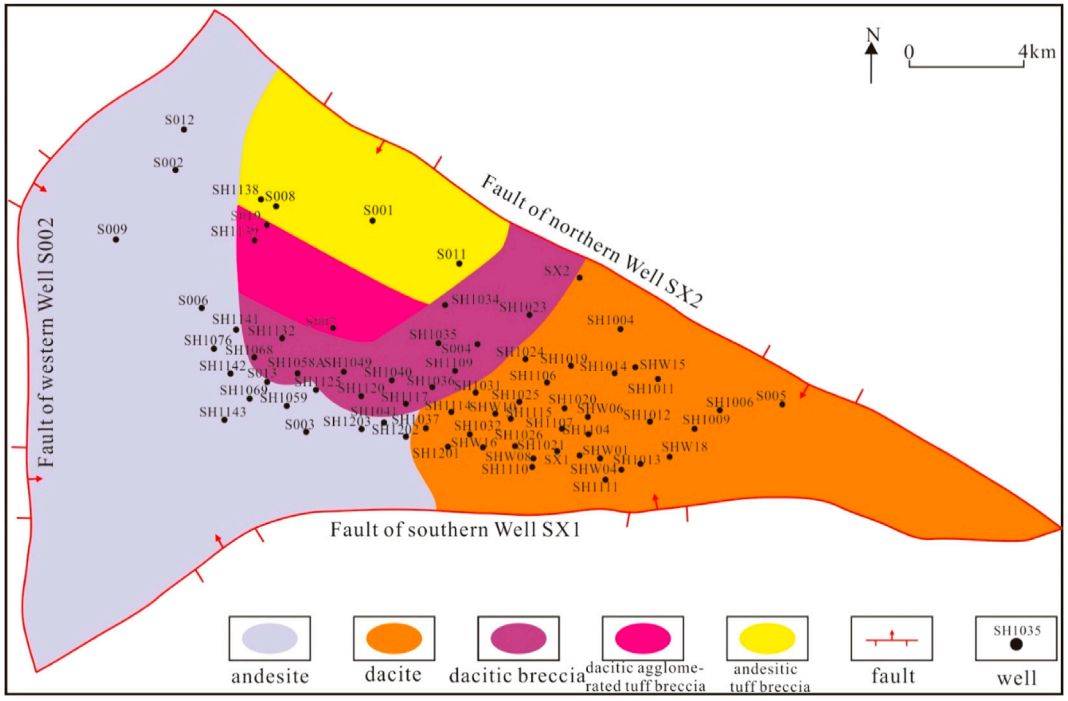


FIGURE 2
Lithology and lithofacies distribution of the Carboniferous volcanic top surface in the Shixi Oilfield.

secondary pores, which are more obvious under a microscope. The volcanic reservoir space in the study area often combines with microcracks to form dissolution-fracture pores (Li J. J. et al., 2022; Fan et al., 2022; Li, 2022; ; Wang et al., 2022).

## 4.2 The "four properties" relations of the reservoir

The "four properties" of the reservoir refer to the reservoir's lithology, physical properties, electrical properties, and oil and gas properties. Among them, the electrical properties constitute the comprehensive response to reservoir lithology, physical properties, and oil and gas properties; of these, lithology is dominant, and the particle size, sorting, cementation type, and argillaceous content directly affect the physical properties of the reservoir (Li et al., 2019b; Mollajan et al., 2013; Zhou et al., 2020; Zhao et al., 2022). Therefore, studying the relationship between these can determine the lower limit of the effective thickness and provide a basis for the final and accurate judgment of the oil and gas stratum.

### 4.2.1 Relationship between lithology and physical properties

The physical properties of different lithologies have obvious differences. Lithologies with relatively ideal physical properties in the study area include breccia lava, banded lava, agglomerate, and compact tuff. The maximum porosity is distributed between 20% and 30%, with an average of approximately 10%. The permeability variation range is between 0.02 and 500 mD, and the average is generally lower than 10 mD. The development of reservoir fractures greatly influences the permeability of different lithologies. In addition, the physical properties of the weathering crust after weathering and leaching are also ideal. At the same time, other lithologies, such as basalt and andesite, have poor physical properties, making it difficult to form effective reservoirs.

The correlation between the lithology and physical properties of the reservoirs in the study area is obvious. The correlation between agglomerate and breccia lava is relatively good, showing the characteristics of high porosity and high permeability, and the banded lava is characterized by high porosity and low permeability. This finding indicates, to some extent, that the degree of development of different lithologic fractures varies greatly. Generally, the correlation between porosity and permeability of the different lithologies in the study area is moderate (Figure 4).

### 4.2.2 Relationship between lithology and oil-bearing properties

The oil-bearing property grade of the core is an important indicator for judging the presence of oil and gas. According to the

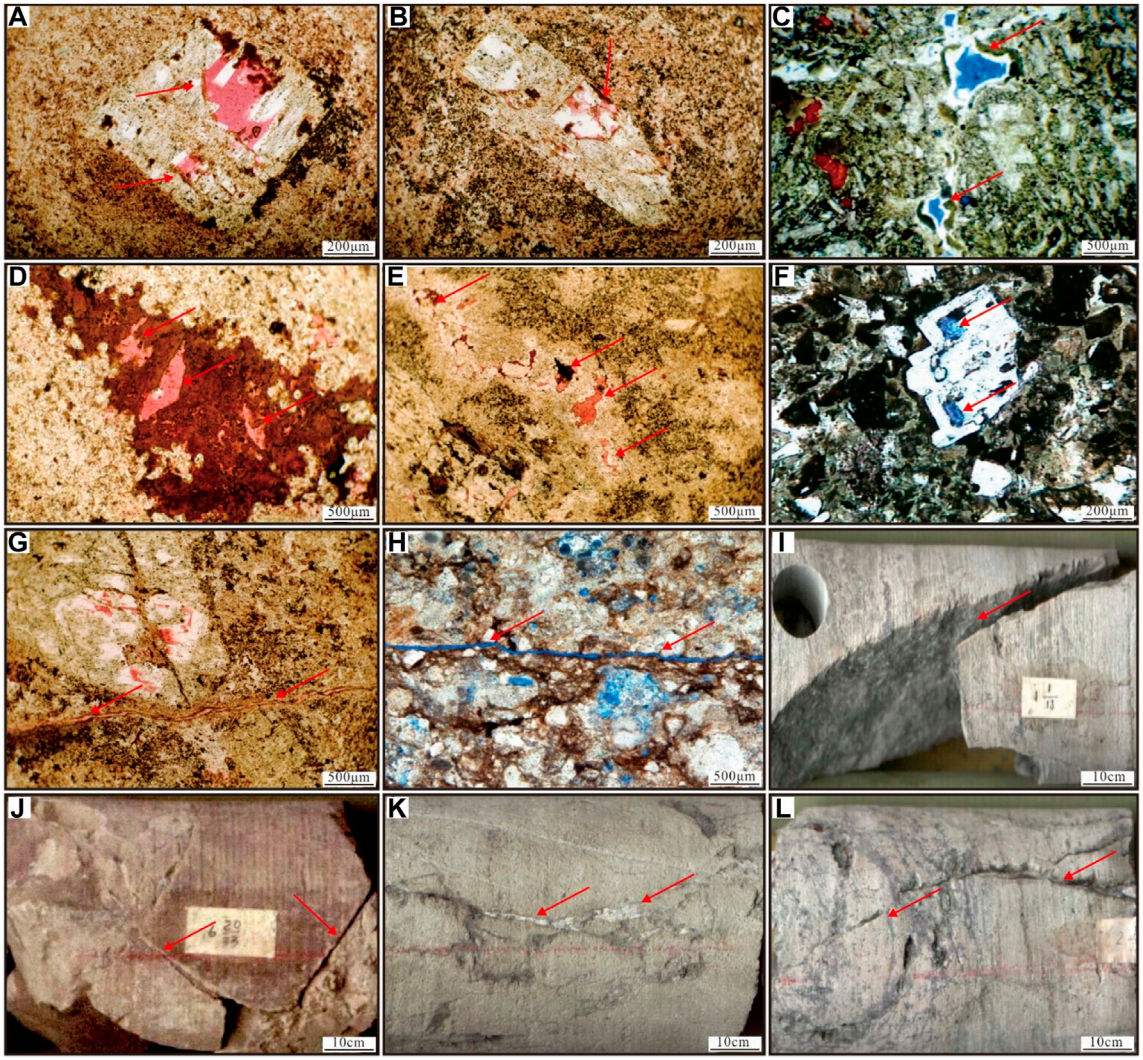


FIGURE 3
Types and characteristics of Carboniferous volcanic rocks reservoir space in Shixi Oilfield. **(A)** Primary pore, S001, 4502.90 m; **(B)** Primary pore, S001, 4501.75 m; **(C)** Intercrystalline pore, S004, 4382.00 m; **(D)** Intercrystalline pore, S001, 4519.97 m; **(E)** Dissolution pore, S001, 4524.50 m; **(F)** Dissolution pore, S004, 4368.70 m; **(G)** Micro shear fracture, S001, 4513.25 m; **(H)** Micro shear fracture, S004, 4392.16 m; **(I)** Shear fracture, S013, 4421.00–4421.10 m; **(J)** Shear fracture, S007, 4352.50 m; **(K)** Tensile fracture, S002, 4412.90 m; **(L)**. Weathering fracture, S013, 4421.10 m.

oil-bearing property analysis of 74 blocks of different lithologies in the study area, the oil- and gas-bearing properties of the cores constitute multiple levels, e.g., gas-bearing, fluorescence (dominant, accounting for 81.1%), oil spot, and oil-rich, while oil-rich samples are rare, accounting for only 1.3% (Figure 5), indicating that the oil-bearing property of Carboniferous reservoirs is average to poor.

### 4.2.3 Relationship between the electrical property and oil-bearing property

This study analyses the electrical properties of the tested oil and gas sections of the main Carboniferous exploration wells (S013, S004, S012, and S002) and clarifies the corresponding relationship between the electrical properties and oil-bearing properties of the reservoir. The research shows that the oil, gas, and water stratum can be explained well by the electrical measurement data (Rt, GR, AC, and DEN) (Table 2), and the test results correspond well to the interpreted electrical properties.

### 4.2.4 Relationship among lithology, physical properties, electrical properties, and oil-bearing property

Based on the above analysis, Carboniferous volcanic reservoirs' agglomerates and breccia lava have good physical properties. The physical properties of the agglomerate change greatly, and fluorescence display is more common; the resistivity

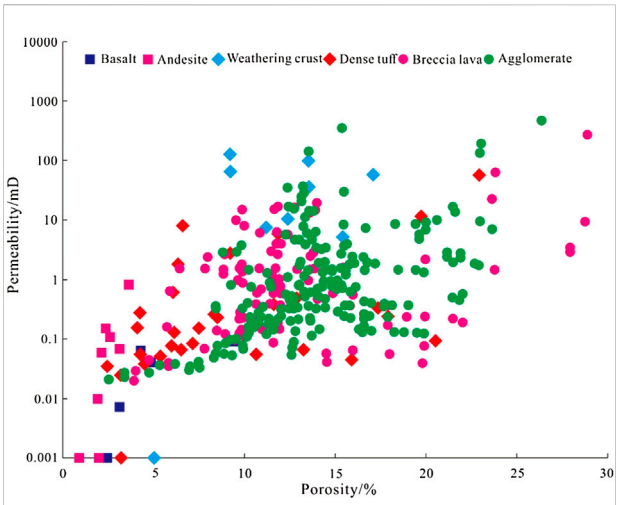


FIGURE 4
Cross plot of porosity and permeability of different lithologies of the Carboniferous system in the Shixi Oilfield.

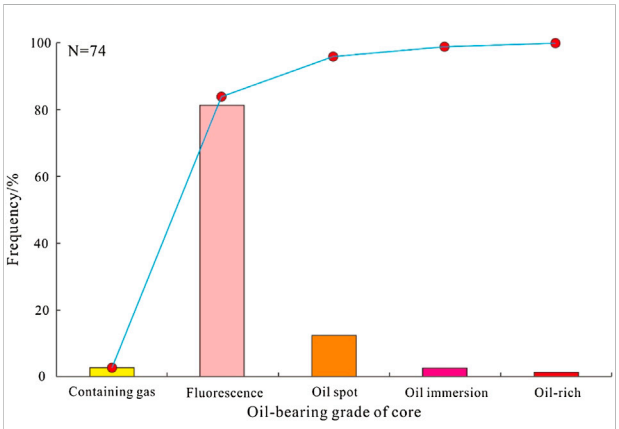


FIGURE 5
Oil-bearing property frequency distribution of the Carboniferous reservoir in the Shixi Oilfield.

shows obvious changes, and the resistivity increases with the increase in oil-bearing properties; when oil and gas are located, the spontaneous potential shows a positive anomaly. The spontaneous potential of the weathering crust is a negative anomaly, with low resistivity, and no oil and gas are found. In general, the lithology, electrical properties, physical properties, and gas-bearing properties of the volcanic reservoirs in the study area have obvious relationships. Lithology affects the physical properties, while physical properties control oil- and gas-bearing properties, and electrical properties respond to the differences and changes in lithology, physical properties, and gas-bearing properties.

## 4.3 Reservoir parameter logging interpretation model

The porosity, permeability, and saturation logging interpretation models are established based on the principle of "core scale logging" and combined with the analysis of the cross-plot and logging curve characteristics (Radwan 2021; He et al., 2021).

### 4.3.1 Physical property parameter logging interpretation model

Physical property parameters include porosity and permeability. In general, calculating porosity using logging parameters, such as acoustic waves, density, and neutrons (Saeid et al., 2022). According to the physical property analysis data for the 12 wells in the study area, the porosity value at each depth corresponds to the logging parameter value, and the acoustic wave-porosity, neutron-porosity, and density-porosity models of Carboniferous volcanic reservoirs are established (Figure 6). The corresponding relationships are illustrated as follows:

$$\varphi = 0.476\mathrm{AC} - 19.121, R^2 = 0.2826 \quad (1)$$

$$\varphi = -38.795DEN + 107.24, R^2 = 0.66 \quad (2)$$

$$\varphi = 0.1056\mathrm{CNL} + 11.55, R^2 = 0.0411 \quad (3)$$

The correlation coefficient R of the acoustic wave-porosity and neutron-porosity models is small, indicating a poor correlation, while the density-porosity model has a good correlation. Therefore, the density-porosity is selected to establish a porosity logging interpretation model. To verify the model's accuracy, well S001 and well S003 were selected for porosity calculation. The calculated results agree with the actual core analysis porosity, and the correlation coefficient exceeded 0.8, indicating that the model is accurate (Figure 7).

Carboniferous volcanic reservoir fractures have developed, making the fracture permeability hundreds of times higher than the matrix permeability. The correlation between rock porosity and the permeability of the fractured reservoir is poor. An effective method to calculate the permeability of fractured reservoirs is still lacking (Jarvie et al., 2007; Ibrahim et al., 2017; Hooker et al., 2018; Hou et al., 2020). Therefore, using conventional logging models to calculate permeability is of little significance.

### 4.3.2 Saturation calculation model

Oil-bearing saturation is the main basis for quantitatively evaluating the oil-bearing property of a reservoir. This parameter is important in describing the reservoir characteristics and is the key to identifying the oil layer. Comprehensively considering the geological properties, rock-electrical experimental parameters, formation water salinity, and other data, the Archie formula was used as the water saturation calculation formula (Eq. 5), establishing the oil saturation formula (Eq. 4).

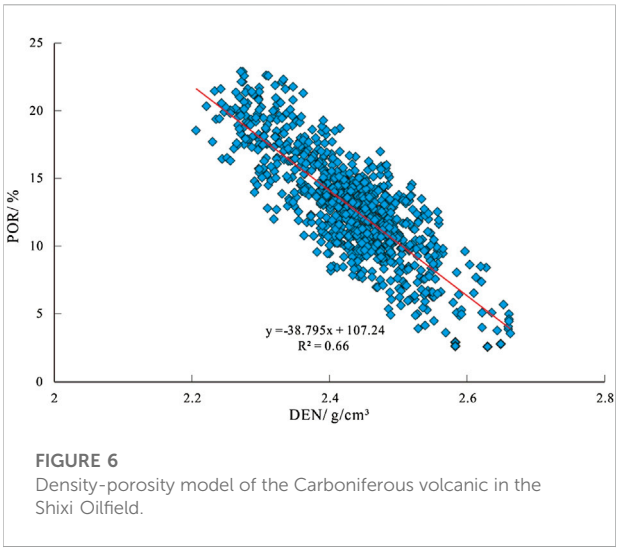


FIGURE 6
Density-porosity model of the Carboniferous volcanic in the Shixi Oilfield.

$$S_w^n = \frac{abR_w}{\varphi^m \times R_t} \quad (4)$$

$$So = 1 - Sw \quad (5)$$

where Sw—water saturation (%); Rt—stratum resistivity (Ω·m); Rw—stratum water resistivity (Ω·m); ф—porosity. The m, n, a, and b values of the study area were obtained from the comprehensive analysis of rock-electrical experiments and previous research results, m=2.13, *n*=1.7, a=0.85, b=1.06, and Rw=0.12 Ω m.

## 4.4 Reservoir fluid identification

Many methods are available for identifying reservoir fluids, including the porosity curve overlapping, cross-plot, and normal probability distribution methods. Regarding volcanic reservoirs,

TABLE 2 Relationship between the electrical property and oil-bearing property of the main exploration well.

| Well | Depth (m) | Rt (Ω.m) | GR (API) | AC (μs/ft) | DEN (g/cm³) | Test | Logging interpretation | Remark |
|---|---|---|---|---|---|---|---|---|
| S013 | 4408–4425 | 14.66–40.08 25.73 | 86.38–131.14 112.36 | 61.51–71.85 65.53 | 2.33–25.0 2.42 | Oil layer | Oil and gas production | A significantly negative difference in spontaneous potential |
| S004 | 4410–4420 | 17.57–51.81 28.31 | 76.42–142.54 109.5 | 55.41–68.71 62.08 | 2.39–2.57 2.5 | Oil-water layer | Oil, gas, and water production | |
| S012 | 4460–4474 | 383.70–1025.82 650.3 | 114.26–126.14 120.27 | 51.90–55.71 53.85 | 2.53–2.60 2.57 | Oil-bearing water layer | Oil-bearing water layer | |
| S002 | 4416–4428 | 7.30–23.65 13.44 | 85.40–134.59 116.3 | 62.65–86.89 70.82 | | Water layer | Water layer | Low resistivity, large interval transit time, and water saturation of 76.55% |
| | 4483–4495 | | | | | | | |
| | 4508–4520 | | | | | | | |

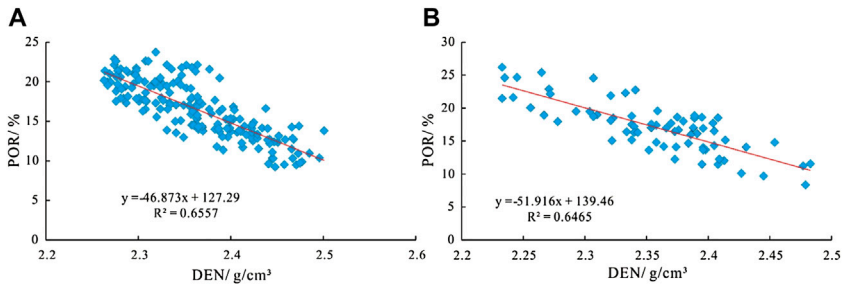


FIGURE 7
The relationship between porosity and density in the study area. **(A)** well S001; **(B)** well S005.

TABLE 3 Accuracy comparison of different fluid identification methods in Carboniferous volcanic reservoirs.

| Well | Depth (m) | Test | Conclusion of explanation | | |
|---|---|---|---|---|---|
| | | | Resistivity-porosity cross-plot | Normal probability distribution | Rt/Rxo-Rt cross-plot |
| S001 | 4442–4454 | Water layer | Oil layer | Water layer | Water layer |
| S002 | 4416–4428 | Water layer | Oil layer | Water layer | Water layer |
| S003 | 4415–4440 | Oil-bearing water layer | Oil-bearing water layer | Oil-bearing water layer | Oil-bearing water layer |
| S004 | 4410–4420 | Oil-water layer | Oil-water layer | Oil layer | Oil-water layer |
| S005 | 4536–4540 | Water layer | Water layer | Oil layer | Oil-water layer |
| S006 | 4437–4443 | Oil-water layer | Oil layer | Oil-bearing water layer | Water layer |
| S007 | 4497–4420 | Oil-water layer | Oil-water layer | Oil-water layer | Water layer |
| S012 | 4460–4474 | Oil-bearing water layer | Oil-bearing water layer | Oil-water layer | Oil layer + Oil-water layer |
| SX2 | 4552–4560 | Dry layer | Dry layer | Water layer | Dry layer |
| S019 | 4420–4440 | Oil layer | Oil layer | Oil layer | Oil-water layer |

the cross-plot and normal probability distribution methods are often used for fluid identification.

### 4.4.1 Resistivity-porosity cross-plot method

Combined with the study on the relations of the "four properties" of the reservoir, the deep lateral resistivity (Rt) of the Carboniferous in the study area corresponds well to the oil-bearing property, and deep lateral logging has a large detection depth and high reliability. When the difference between lithology and physical properties of the reservoir is small, the resistivity increases, indicating the possible presence of an oil and gas stratum, though possibly a water stratum instead. In the meantime, the deep lateral resistivity and porosity cross-plot can also be used to judge the quality of physical properties to a certain extent. The porosity of the dry stratum is smaller than that of the oil and water strata. In addition, the dry and oil strata are easily distinguished, and the limit value between them is Φ=10% (Figure 8). The fluid properties of the reservoir are identified by the resistivity-porosity log cross-plot method, with the coincidence rate reaching 80% (Table 3).

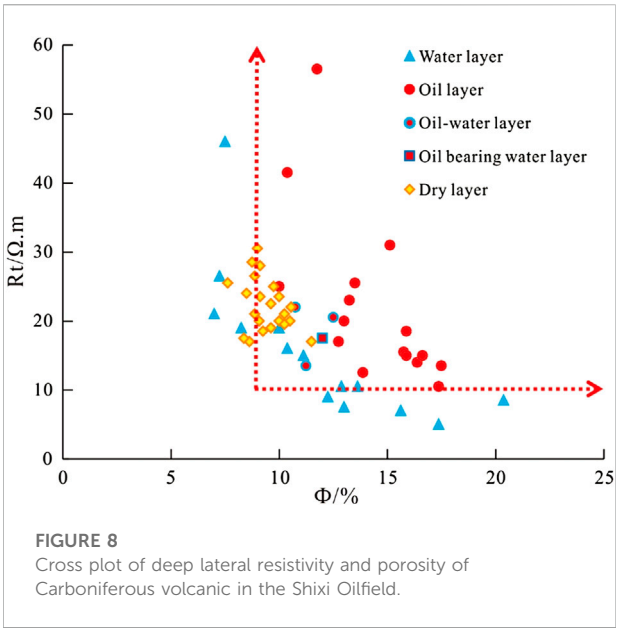


FIGURE 8
Cross plot of deep lateral resistivity and porosity of Carboniferous volcanic in the Shixi Oilfield.

### 4.4.2 Normal probability distribution method ($P^{1/2}$ method)

Normal probability distribution method is a mathematical statistical method for reservoir fluid identification. A normal probability distribution map was drawn to analyze the fluid properties using the test data for the main single well in the study area (Figure 9). The oil stratum k>0.009; the water stratum k<0.004; the electrical properties of the oil-water and oil-bearing water strata were very similar, with k ranging from 0.004 to 0.009; making it difficult to distinguish such fluid types using the normal probability distribution method. Similarly, using the single-well test data and interpretation results to compare, the coincidence rate of the normal probability distribution method for judging fluid properties is approximately 65% (Table 3).

### 4.4.3 Rt/Rxo-Rt cross-plot method

The cross-plot of Rt/Rxo and Rt can better identify the fluid properties of different reservoir types (Das and Chatterjee, 2018). Different fluids in the study area mainly show the following rules in the cross-plot of Rt/Rxo and Rt (Figure 10): 1) Oil stratum: resistivity is greater than 37 Ω m, and the ratio is greater than 1.6; 2) Oil-water and oil-bearing water strata: resistivity is 19–35 Ω m, and the ratio is between 0.7 and 2.2; water stratum: resistivity is lower than 30 Ω m, and the ratio is

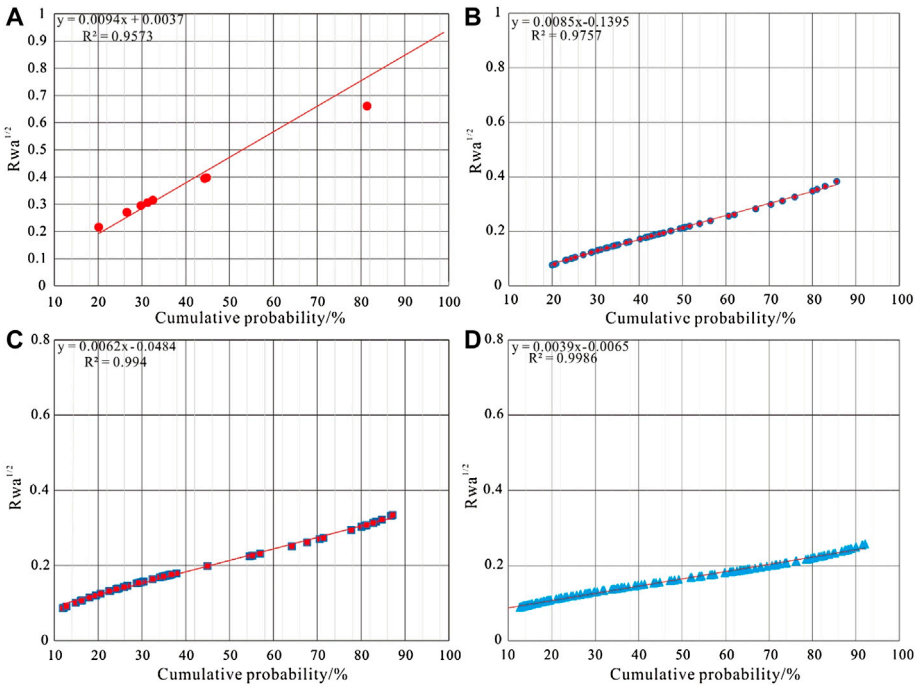


FIGURE 9
Normal probability distribution of the study area. **(A)** oil layer; **(B)** oil-water layer; **(C)** oil-bearing water layer; **(D)** water layer.

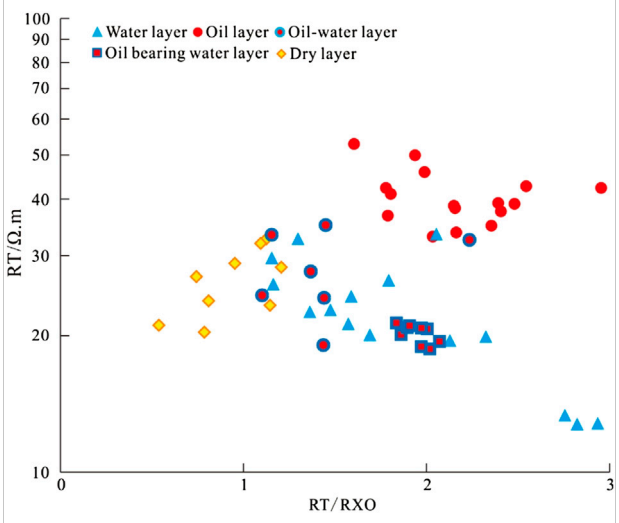


FIGURE 10
Rt/Rxo and Rt cross-plot of the Carboniferous volcanic in the Shixi Oilfield.

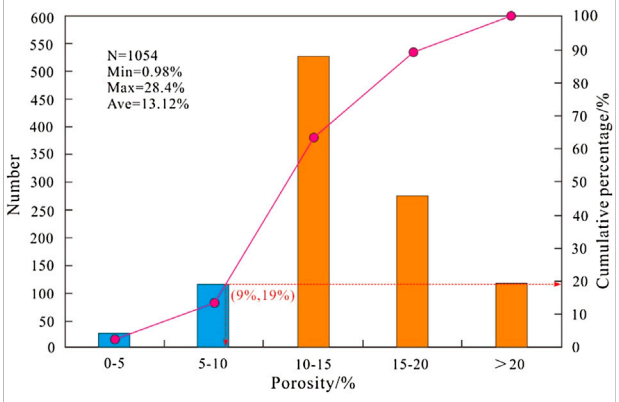


FIGURE 11
The lower limit of porosity of the Carboniferous volcanic in the Shixi Oilfield.

between 1.0 and 3.0; dry stratum: resistivity is 19–35 Ω m, and the ratio is between 0.5 and 1.2. Since the oil-water stratum and the oil-water stratum have similar electrical properties, they are combined for analysis. This method can better identify oil, water, and dry strata; however, distinguishing between oil-water and oil-bearing water strata is difficult. Similarly, using the single-well test data and interpretation results as a comparison, the coincidence rate of this method for judging fluid properties is approximately 63.63% (Table 3).

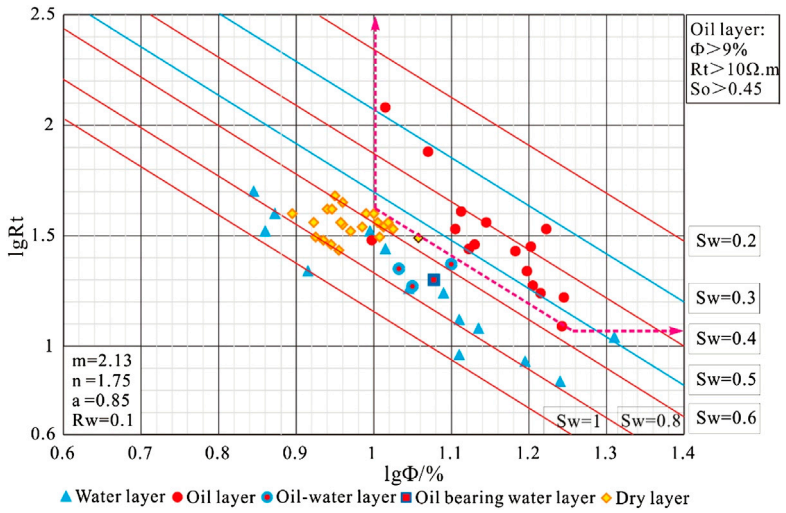


FIGURE 12
The cross plot of resistivity-porosity of the Carboniferous volcanic in the Shixi Oilfield.

TABLE 4 Statistics of oil and water stratum interpretation criteria.

| Description | Oil layer | Oil-water layer (oil-bearing water layer) | Water layer | Dry layer |
|---|---|---|---|---|
| Rt (Ω.m) | >10 | (12,24) | >4 | (13,32) |
| POR (%) | >9 | >10 | >9 | <10 |
| So (%) | >45 | (20,45) | <40 | — |

# 5 Discussion

## 5.1 Determination of the lower limits of the reservoirs

In general, the lower limits of the reservoir include two types such as that of physical properties and oil/gas saturation. This study determines the lower limit of physical properties based on the core physical property analysis data, combined with the oil and gas display. According to the oil and gas display and measured physical property data for the 12 wells, such as S005, S013, and S019, the porosity of 9% and the permeability of 0.2 mD have been determined as the lower limits of the physical properties of Carboniferous reservoirs (Figure 11).

The lower limit of oil saturation is also the upper limit of water saturation. Using the oil test, perforation, and logging data for the Carboniferous oil strata, a resistivity-porosity cross-plot is drawn, and the oil strata, oil-water strata, oil-bearing water strata, and water strata boundaries are demarcated based on the different distributions of them on the plate. Therefore, the lower limit of oil saturation of Carboniferous reservoirs in the study area is 45% (Figure 12).

## 5.2 Reservoir fluid identification criteria

In this study, three commonly used methods were selected to identify the fluid properties of Carboniferous volcanic reservoirs, and the coincidence rates of resistivity-porosity cross-plot, normal probability distribution, and Rt/Rxo-Rt cross-plot method were 80%, 63.63%, and 63.63%, respectively. The identification accuracy of different methods differs due to the particularity of volcanic reservoirs and the adaptability of the methods. The resistivity-porosity cross-plot method is suitable for areas where drilling fluid does not intrude deeply into the stratum, and the reservoir porosity is relatively high, and it can better divide dry, oil, and water strata. The normal probability distribution method identifies fluids using the combination of apparent stratum water resistivity and mathematical theory. This method applies to pore-type and

fracture-pore-type reservoirs, provided that the difference in stratum water resistivity is small. The Rt/Rxo-Rt cross-plot method is mainly suitable for the division of oil and water strata according to the different fluid properties corresponding to different reservoir types, while the applicability to oil-water and oil-containing water strata is poor. Therefore, the resistivity-porosity cross-plot method is used for fluid identification in the study area with high accuracy, but it is still necessary to combine multiple methods for mutual verification to better identify the fluid properties of volcanic reservoirs. Based on the above analysis, this study summarizes the oil-water stratum identification criteria for volcanic reservoirs in the study area based on the research on oil and gas displays, test data, conventional logging response characteristics, fluid identification methods, and reservoir lower limits (Table 4).

## 6 Conclusion

1) The lithofacies of Carboniferous volcanic in the Shixi Oilfield include explosive and effusive facies, with the latter dominating. The lithology is mainly breccia lava, agglomerate, banded lava, and compact tuff. The main types of reservoir space are secondary pores and tectonic fissures. The tectonic fissures are of great significance to the improvement of reservoir properties. The corrosion-fracture pores that connect with primary and secondary pores are important reservoir spaces. The physical properties of the reservoir matrix are characterized by medium-high porosity and low permeability and belong to the fracture-pore reservoir with medium-high porosity and low permeability overall.
2) The lithology, electrical properties, physical properties, and gas-bearing properties of the volcanic reservoirs in the study area have obvious relationships. Lithology affects physical properties, which control oil- and gas-bearing and electrical properties, all of which have obvious responses to the differences and changes in lithology, physical properties and gas-bearing properties. Thus, a logging interpretation model applicable to the volcanic reservoir's physical parameters and oil saturation in the study area has been established.
3) The fluid identification criteria for volcanic reservoirs were established based on three methods, among which the resistivity-porosity cross-plot method has the best identification effect, with a coincidence rate of 80%. Given the shortcomings of the different methods, mutual verification based on multiple methods is the key to accurately identifying reservoir fluids. Using the reservoir parameter logging interpretation model and fluid identification plate, the lower porosity, permeability, and oil saturation limits are 9%, 0.2 mD, and 45%, respectively. Based on the characteristics of volcanic rock lithology and lithofacies, this paper comprehensively applied various fluid identification methods to improve the identification accuracy, and effectively guided the exploration and development of volcanic oil and gas in this area.

## Data availability statement

The original contributions presented in the study are included in the article/supplementary material, further inquiries can be directed to the corresponding author.

## Author contributions

LF, ZQ, AX, LC, Junfei Li, NW contributed in writing, reviewing, and editing, datacuration, writing—original draft preparation; QQ, KM contributed in formal analysis, validation, and reviewing.

## Acknowledgments

We thank all editors and reviewers for their helpful comments and suggestions.

## Conflicts of interest

LF, JL, NW were employed by the Shixi Field Operation District, Xinjiang Oilfield Company, CNPC, ZQ was employed by the Exploration Division, Petro China Southwest Oil and Gasfield Company, AX was employed by the Evaluation Department of Xinjiang Oilfield Company, CNPC, and LC was employed by Development Department of Xinjiang Oilfield Company, CNPC.

The remaining authors declare that the research was conducted in the absence of any commercial or financial relationships that could be construed as a potential conflict of interest.

## Publisher's note

# References

Ajaz, M., Ouyang, F., Wang, G. H., Liu, S. L., Wang, L. X., and Zhao, J. G. (2021). Fluid identification and effective fracture prediction based on frequency-dependent AVOAz inversion for fractured reservoirs. *Pet. Sci.* 18 (4), 1069–1085. doi:10.1016/j.petsci.2021.07.011

Chen, Z. Y., Yan, H., Li, J. S., Zhang, G., Zhang, Z. W., and Liu, B. Z. (1999). Relationship between Tertiary volcanic rocks and hydrocarbons in the Liaohe basin, People's Republic of China. *AAPG Bull.* 83 (6), 1004–1014. doi:10.1306/E4FD2E51-1732-11D7-8645000102C1865D

Das, B., and Chatterjee, R. (2018). Well log data analysis for lithology and fluid identification in Krishna-Godavari Basin, India. *Arab. J. Geosci.* 11 (10), 231. doi:10.1007/s12517-018-3587-2

Fan, C. H., Xie, H. B., Li, H., Zhao, S. X., Shi, X. C., Liu, J. F., et al. (2022). Complicated fault characterization and its influence on shale gas preservation in the southern margin of the Sichuan Basin, China. *Lithosphere*, 2022 8035106. doi:10.2113/2022/8035106

Fan, C. H., Li, H., Qin, Q. R., He, S., and Zhong, C. (2020b). Geological conditions and exploration potential of shale gas reservoir in Wufeng and Longmaxi Formation of southeastern Sichuan Basin, China. *J. Pet. Sci. Eng.* 191, 107138. doi:10.1016/j.petrol.2020.107138

Fan, C. H., Li, H., Qin, Q. R., Shang, L., Yuan, Y. F., and Li, Z. (2020a). Formation mechanisms and distribution of weathered volcanic reservoirs: A case study of the carboniferous volcanic rocks in northwest Junggar Basin, China. *Energy Sci. Eng.* 8 (8), 2841–2858. doi:10.1002/ese3.702

Feng, Z. Q. (2008). Volcanic rocks as prolific gas reservoir: A case study from the qingshen gas field in the songliao basin, NE China. *Mar. Pet. Geol.* 25 (4/5), 416–432. doi:10.1016/j.marpetgeo.2008.01.008

He, M., Gu, H. M., and Wan, H. (2020). Log interpretation for lithology and fluid identification using deep neural network combined with MAHAKIL in a tight sandstone reservoir. *J. Pet. Sci. Eng.* 194, 107498. doi:10.1016/j.petrol.2020.107498

He, S., Li, H., Qin, Q. R., and Long, S. X. (2021). Influence of mineral compositions on shale pore development of longmaxi formation in the dingshan area, southeastern sichuan basin. China. *Energy fuels* 35 (13), 10551–10561. doi:10.1021/acs.energyfuels.1c01026

Hooker, J. N., Abu-Mahfouz, I. S., Meng, Q., and Cartwright, J. (2018). Fractures in mudrocks: Advances in constraining timing and understanding mechanisms. *J. Struct. Geol.* 125, 166–173. doi:10.1016/j.jsg.2018.04.020

Hou, E. K., Cong, T., Xie, X. S., and Wei, J. B. (2020). Ground surface fracture development characteristics of shallow double coal seam staggered mining based on particle flow. *J. Min. Strata Control Eng.* 2 (1), 013521. doi:10.13532/j.jmsce.cn10-1638/td.2020.01.002

Hou, L. H., Luo, X., Wang, J. H., Yang, F., Zhao, X., and Mao, Z. G. (2013). Weathered volcanic crust and its petroleum geologic significance: A case study of the carboniferous volcanic crust in northern Xinjiang, NW China. *Pet. explor. Dev.* 40 (3), 277–286. doi:10.1016/S1876-3804(13)60034-8

Hou, L. H., Zou, C. N., Liu, L., Wen, B. H., Wu, X. Z., Wei, Y. Z., et al. (2012). Geologic essential elements for hydrocarbon accumulation within Carboniferous volcanic weathered crusts in northern Xinjiang, China. *Acta Pet. Sin.* 33 (4), 533–540. doi:10.7623/syxb201204001

Ibrahim, M. I. M., Hariri, M. M., Abdullatif, O. M., Makkawi, M. H., and Elzain, H. (2017). Fractures system within Qusaiba shale outcrop and its relationship to the lithological properties, Qasim area, Central Saudi Arabia. *J. Afr. Earth Sci.* 133, 104–122. doi:10.1016/j.jafrearsci.2017.05.011

Jarvie, D. M., Hill, R. J., Ruble, T. E., and Pollastro, R. M. (2007). Unconventional shale-gas systems: The Mississippian Barnett Shale of north-central Texas as one model for thermogenic shale-gas assessment. *Am. Assoc. Pet. Geol. Bull.* 91 (4), 475–499. doi:10.1306/12190606068

Kang, H. P. (2021). Temporal scale analysis on coal mining and strata control technologies. *J. Min. Strata Control Eng.* 3 (1), 013538. doi:10.13532/j.jmsce.cn10-1638/td.20200814.001

Li, H., Qin, Q. R., Li, Z. J., Fan, C. H., Zhong, K., Li, Z., et al. (2017). Characteristics and distribution of cracks in Carboniferous buried volcanic reservoirs of the Shixi Oilfield. *Geol. Expl.* 53 (6), 1219–1228. doi:10.13712/j.cnki.dzykt.2017.06.018

Li, H., Tang, H. M., Qin, Q. R., Fan, C. H, Han, S., Yang, C., et al. (2018). Reservoir characteristics and hydrocarbon accumulation of Carboniferous volcanic weathered crust of Zhongguai high area in the western Junggar Basin, China. *J. Cent. South Univ.* 25 (11), 2785–2801. doi:10.1007/s11771-018-3953-y

Li, H., Tang, H. M., Qin, Q. R., Wang, Q., and Zhong, C. (2019a). Effectiveness evaluation of natural fractures in Xujiahe Formation of Yuanba area, Sichuan basin, China. *Arab. J. Geosci.* 12 (6), 194. doi:10.1007/s12517-019-4292-5

Li, H., Tang, H. M., and Zheng, M. J. (2019b). Micropore structural heterogeneity of siliceous shale reservoir of the Longmaxi Formation in the southern Sichuan Basin, China. *Minerals* 9, 548. doi:10.3390/min9090548

Li, H., Qin, Q. R., Zhang, B. J., Ge, X. Y., Hu, X., Fan, C. H., et al. (2020). Tectonic fracture formation and distribution in ultradeep marine carbonate gas reservoirs: A case study of the maokou formation in the jiulongshan gas field, sichuan basin, southwest China. *Energy fuels* 34 (11), 14132–14146. doi:10.1021/acs.energyfuels.0c03327

Li, H. (2022). Research progress on evaluation methods and factors influencing shale brittleness: A review. *Energy Rep.* 8, 4344–4358. doi:10.1016/j.egyr.2022.03.120

Li, H., Tang, H. M., Qin, Q. R., Zhou, J. L., Qin, Z. J., Fan, C. H., et al. (2019). Characteristics, formation periods and genetic mechanisms of tectonic fractures in the tight gas sandstones reservoir: A case study of xujiahe formation in YB area, sichuan basin, China. *J. Pet. Sci. Eng.* 178, 723–735. doi:10.1016/j.petrol.2019.04.007

Li, H., Wang, Q., Qin, Q. R., and Ge, X. Y. (2021). Characteristics of natural fractures in an ultradeep marine carbonate gas reservoir and their impact on the reservoir: A case study of the maokou formation of the jls structure in the sichuan basin, China. *Energy fuels* 35 (16), 13098–13108. doi:10.1021/acs.energyfuels.1c01581

Li, J. J., Qin, Q. R., Li, H., Zhao, S. X., and Wan, Y. F. (2022). Numerical simulation of the stress field and fault sealing of complex fault combinations in Changning area, Southern Sichuan Basin, China. *Energy Sci. Eng.* 10 (2), 278–291. doi:10.1002/ese3.1044

Li, J., Li, H., Yang, C., Wu, Y. J., Gao, Z., and Jiang, S. L. (2022). Geological characteristics and controlling factors of deep shale gas enrichment of the Wufeng-Longmaxi Formation in the southern Sichuan Basin, China. *Lithosphere* 2022, 4737801. doi:10.2113/1970/4737801

Li, X., Fu, L., Ji, J. Q., Xie, L., Zhang, J. L., Li, H., et al. (2022). Reservoir characteristics and accumulation analysis of carboniferous volcanic rocks in Shixi Oilfield, Junggar Basin, China. *Chin. J. Geol.* 57 (3), 704–719. doi:10.12017/dzkx.2022.041

Liu, Z. Y., Pan, Z. J., Li, S. B., Zhang, L. G., Wang, F. S., Wang, C. H., et al. (2022). Fracturing optimization design of fractured volcanic rock in songliao basin based on numerical research and orthogonal test. *Lithosphere* 2022, 3325935. doi:10.2113/2022/3325935

Mollajan, A., Memarian, H., and Tokhmechi, B. (2013). Proposing a new integral method for fluid type identification from petrophysical logs in a carbonate reservoir. *Energy Explor. Exploitation* 31 (6), 895–908. doi:10.1260/0144-5987.31.6.895

Pan, X. P., Zhang, G. Z., and Yin, X. Y. (2019). Linearized amplitude variation with offset and azimuth and anisotropic poroelasticity. *Geophys. Prospect.* 67 (7), 1882–1897. doi:10.1111/1365-2478.12778

Qie, L., Shi, Y. N., and Liu, J. G. (2021). Experimental study on grouting diffusion of gangue solid filling bulk materials. *J. Min. Strata Control Eng.* 3 (2), 023011. doi:10.13532/j.jmsce.cn10-1638/td.20201111.001

Radwan, A. E. (2021). Modeling pore pressure and fracture pressure using integrated well logging, drilling based interpretations and reservoir data in the giant El Morgan oil field, Gulf of Suez, Egypt. *J. Afr. Earth Sci.* 178, 104165. doi:10.1016/j.jafrearsci.2021.104165

Saeid, E., Kendall, C., Kellogg, J., De Keyser, T., Hafiz, I., Albesher, Z., et al. (2022). A depositional model for the Carbonera Formation, Llanos Foothills, Colombia, from workflow of a sequence stratigraphic framework and interpretation from well-log stacking patterns, well cuttings, and three-dimensional seismic spectral decomposition. *Am. Assoc. Pet. Geol. Bull.* 106 (2), 321–353. doi:10.1306/08092118015

Shan, S. C., Wu, Y. Z., Fu, Y. K., and Zhou, P. H. (2021). Shear mechanical properties of anchored rock mass under impact load. *J. Min. Strata Control Eng.* 3 (4), 043034. doi:10.13532/j.jmsce.cn10-1638/td.20211014.001

Smeraglia, L., Mercuri, M., Tavani, S., Pignalosa, A., Kettermann, M., Billi, A., et al. (2021). 3D Discrete Fracture Network (DFN) models of damage zone fluid corridors within a reservoir-scale normal fault in carbonates: Multiscale approach using field data and UAV imagery. *Mar. Pet. Geol.* 126, 104902. doi:10.1016/j.marpetgeo.2021.104902

Wang, J., and Wang, X. L. (2021). Seepage characteristic and fracture development of protected seam caused by mining protecting strata. *J. Min. Strata Control Eng.* 3 (3), 033511. doi:10.13532/j.jmsce.cn10-1638/td.20201215.001

Wang, S. L., Li, H., Lin, L. F., and Yin, S. (2022). Development characteristics and finite element simulation of fractures in tight oil sandstone reservoirs of Yanchang Formation in western Ordos Basin. *Front. Earth Sci.* 9, 823855. doi:10.3389/feart.2021.823855

Weng, K., Ma, Z. P., Cao, K., Dong, Y. P., Chen, B., and Zhao, X. J. (2020). Petrogenesis and tectonic implications of the early Carboniferous volcanic rocks in West Junggar, NW China. *Geol. J.* 55 (3), 1826–1848. doi:10.1002/gj.3604

Yang, Y. Q., Qiu, L. W., Cao, Y. C., Chen, C., Lei, D. W., and Wan, M. (2017). Reservoir quality and diagenesis of the permian lucaogou formation tight carbonates in jimsar sag, Junggar Basin, west China. *J. Earth Sci.* 28, 1032–1046. doi:10.1007/s12583-016-0931-6

Zhang, H., Ni, H. J., Wang, Z. Z., Liu, S. B., and Liang, H. J. (2020). Optimization and application study on targeted formation ROP enhancement with impact drilling modes based on clustering characteristics of logging. *Energy Rep.* 6, 2903–2912. doi:10.1016/j.egyr.2020.10.020

Zhao, B., Li, Z. P., Gao, C. Q., and Tang, Y. (2022). Identification of complex fluid properties in condensate gas reservoirs based on gas-oil ratio parameters calculated by optimization mathematical model. *Front. Energy Res.* 10, 863776. doi:10.3389/fenrg.2022.863776

Zhou, Y. H., Hu, Q. X., Liu, W. T., Wu, Z. Q., Yan, Y. L., and Ma, J. L. (2020). Study on the origin and fluid identification of low-resistance gas reservoirs. *Geofluids* 2020, 1–12. doi:10.1155/2020/8859309

Zou, C. N., Hou, L. H., Tao, S. Z., Yuan, X. J., Zhu, R. K., Zhang, X. X., et al. (2012). Hydrocarbon accumulation mechanism and structure of large-scale volcanic weathering crust of the Carboniferous in Northern Xinjiang, China. *Sci. China Earth Sci.* 55, 221–235. doi:10.1007/s11430-011-4297-8